

---

# ALBERTA WELLS DATASET: PINPOINTING OIL AND GAS WELLS FROM SATELLITE IMAGERY

---

**Pratinav Seth\***

Mila – Quebec AI Institute  
Manipal Institute of Technology

**Michelle Lin\***

Mila – Quebec AI Institute  
Université de Montréal

**Brefo Dwamena Yaw**

Mila – Quebec AI Institute

**Jade Boutot, Mary Kang**

McGill University

**David Rolnick**

Mila – Quebec AI Institute  
McGill University

## ABSTRACT

Millions of abandoned oil and gas wells are scattered across the world, leaching methane into the atmosphere and toxic compounds into the groundwater. Many of these locations are unknown, preventing the wells from being plugged and their polluting effects averted. Remote sensing is a relatively unexplored tool for pinpointing abandoned wells at scale. We introduce the first large-scale benchmark dataset<sup>1</sup> for this problem, leveraging medium-resolution multi-spectral satellite imagery from Planet Labs. Our curated dataset comprises over 213,000 wells (abandoned, suspended, and active) from Alberta, a region with especially high well density, sourced from the Alberta Energy Regulator and verified by domain experts. We evaluate baseline algorithms<sup>2</sup> for well detection and segmentation, showing the promise of computer vision approaches but also significant room for improvement.

## 1 Introduction

Across the world, there are millions of abandoned oil and gas wells left to degrade by the companies or individuals that built them. No longer producing usable fossil fuels, these wells nonetheless have a significant impact on the environment, with many of them leaking significant quantities of methane, a powerful greenhouse gas, into the atmosphere. In aggregate, these emissions represent the equivalent of millions of tons of carbon dioxide per year [1]. In Canada, an estimated 370,000 abandoned wells produce methane equivalent to half a million metric tons of CO<sub>2</sub> annually [1, 2], while in the U.S., there are an estimated 4 million abandoned wells [1], releasing over five million metric tons of CO<sub>2</sub> equivalent emissions per year.

Despite the small percentage, the high global warming potential of methane underscores the need for improved monitoring and management to reduce environmental impact. Abandoned wells also pose health and safety concerns, in particular by leaching toxic chemicals into the groundwater of surrounding communities [3]. It is possible to plug abandoned wells to mitigate the harms associated with them (with so-called “super-emitter” wells an especially high priority [4, 5]). However, a significant fraction of abandoned wells remain unknown. In Pennsylvania, as much as 90% of abandoned wells are estimated to be unrecorded [5]. In Canada, abandoned wells have been described as the most uncertain source of methane emissions nationally due to the poor quality of data surrounding them [1].

With the advent of large-scale remote sensing datasets and powerful machine learning tools to process them, it has become possible to label and monitor the built environment as never before [6]. Many such works have focused

---

\*Denotes co-first authorship. Correspondence to [seth.pratinav@gmail.com](mailto:seth.pratinav@gmail.com)

<sup>1</sup>Dataset available at: <https://zenodo.org/records/13743323>

<sup>2</sup>Code will be available at: [https://github.com/RolnickLab/Alberta\\_Wells\\_Dataset](https://github.com/RolnickLab/Alberta_Wells_Dataset)

on opportunities to use remote sensing to accelerate climate action and environmental protection, and oil and gas infrastructure has increasingly been an object of scrutiny (see e.g. [7, 8]).

In this work, we present the first large-scale machine-learning benchmark dataset for pinpointing onshore oil and gas wells, encompassing abandoned, suspended, and active wells. Our main contributions are as follows:

- We introduce the Alberta Wells Dataset, containing information on over 200k abandoned, suspended, and active onshore oil and gas wells with high-resolution satellite imagery.
- We frame the problem of identification of wells as a challenge for object detection and binary segmentation.
- We evaluate a wide range of state-of-the-art deep learning algorithms, showing promising performance but emphasizing the challenging nature of the task.

We hope that this work will represent a step towards scalable identification of abandoned well sites and the reduction of their deleterious effects on our climate and environment.

## 2 Previous Work

Hundreds of satellites continuously monitor the Earth’s surface, generating petabyte-scale remote sensing datasets [6]. With advancements in hardware, the quality of remote sensing images has significantly improved in terms of spatial and temporal resolution. High-quality remote sensing data are available through state-funded projects like Sentinel and Landsat, and more recently through private enterprises such as Planet Labs [9].

Increasingly, machine learning has been used to parse such raw data, including in a wide range of applications for tackling climate change [7]. Benchmark datasets in this area have included tasks in land use and land cover (LULC) estimation [10], crop classification [11, 12], species distribution modeling [13], and forest monitoring [14]. Some datasets like SpaceNet 7 [15] include a few cases of study sites with oil wells, although the dataset was developed for multi-temporal urban monitoring.

Within this area of research, an increasing body of work has considered the problem of detecting artifacts associated with oil and gas operations. The detection of oil spills using a combination of remote sensing and machine learning has been widely explored [16, 17, 18]. Recently, the detection of oil and gas infrastructure has also been investigated [8, 19], with some studies focusing on the goal of estimating methane emissions [20, 21]. The dataset by [8] includes 7,066 aerial images, with 149 images of oil refineries. The METER-ML dataset [20] comprises 86,599 georeferenced images in the U.S. labeled for methane sources. The OGIM v1 dataset [21] includes 2.6 million point locations of major facilities. A dataset by [22] features 1,388 images of pipelines in the Arctic, while a dataset by [23] includes 3,266 images of heavy-polluting enterprises with 0.25 m resolution.

The problem of detection of oil and gas wells has also been proposed by a number of authors. Existing datasets, however, are quite small (500-10,000 samples) and typically are limited to a small region and contain only active wells, limiting their applicability in the context of identifying abandoned or suspended wells as summarized in Table 1. Most of these studies have primarily focused on basic machine learning algorithms for well detection due to the limited sample size.

Table 1: Previous datasets in which remote sensing algorithms are applied to detect oil and gas wells. “N/A” is given for datasets that do not indicate the number of individual wells in the dataset.

Dataset	O&G Well Count	Total Well Images	Resolution (m/px)	Geography	Imagery Source
NEPU-OWOD V1.0 [24]	1,192	432	0.41	Daqing City, China	Google Earth
NEPU-OWOD V3.0 [25]	3,749	722	0.48	China & California	
Oil Well Dataset [26]	N/A	5,895	0.26	Daqing City, China	
O&G Infrastructure [27]	630	930	0.15 - 1	Permian Basin, USA	
Well Pad Dataset [28]	12,490	10,432	0.3-0.7	Permian and Denver Basins, USA	
NEPU-OWS V1.0 [29]	N/A	1,200	10	Russia	Sentinel-2
NEPU-OWSV2.0 [30]	N/A	120	10/20/60	Austin, USA	
<b>Alberta Well Dataset (Ours)</b>	<b>213,447</b>	<b>94,343</b>	3	Alberta, Canada	Planet Labs

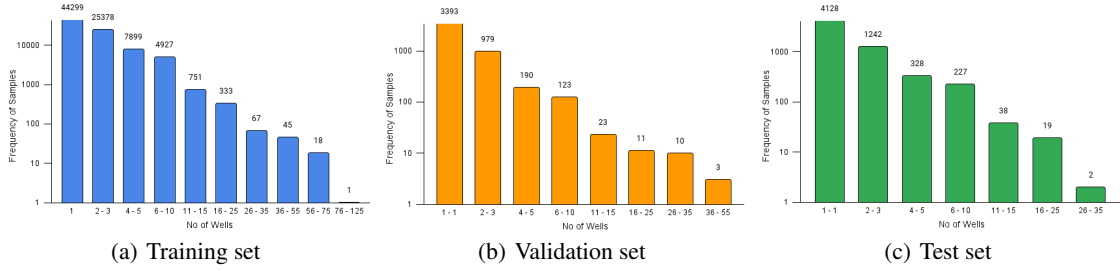


Figure 1: Distribution of the number of individual wells in positive samples from the dataset. We also include an equal number of images with no wells at all.

### 3 Alberta Wells Dataset

We introduce the Alberta Wells Dataset for oil and gas well detection. The dataset is drawn from the province of Alberta, Canada, a region with the third-largest oil reserves in the world and a substantial number of oil and gas wells, many of which have been present for over a century. The entire province of Alberta (an area larger than the UK and Germany combined) encompasses a diverse range of geographical zones and is highly diverse for a landlocked region, including prairies, lakes, forests, and mountains. The dataset contains over 188,000 patches of satellite imagery acquired by Planet Labs [9], which we make publicly available, with around 94,000 containing wells covering more than 213,000 individual wells. Each patch is annotated with labels for both segmentation and bounding box localization. The annotations are based on data from the Alberta Energy Regulator [31], quality-controlled by domain experts.

Our dataset attempts to maximize the amount of data available for learning by including a mixture of active and suspended wells alongside abandoned wells. These types of wells appear overall similar in satellite imagery. In contrast to abandoned wells, “suspended” refers to wells that have merely paused operations temporarily, though this designation can be inaccurate, and some wells are classified as suspended for long enough that they are truly abandoned. Active wells are those that are currently in operation.

To simulate real-world conditions, we ensure a varied density of wells per image, as highlighted in Figure 1. We also include satellite imagery patches with no wells present from areas nearby to areas with wells, ensuring no overlap between the samples. This balanced dataset maintains an equal distribution of well and non-well images. Table 2 details the total sample count in each dataset split. It also mentions the count of oil wells in active, abandoned, and suspended states in each dataset split, emphasizing the dataset’s comprehensive nature.

#### 3.1 Data Collection, Quality Control & Patch Creation

The Alberta Energy Regulator (AER) oversees the energy industry in the province, ensuring companies adhere to regulations as they develop oil and gas resources. AER publishes AER ST37 [31], a monthly list of all wells reported in Alberta, detailing their geographic location, mode of operation, license status, and type of product being extracted, among other attributes. This data provides a metadata (.txt) file and a .shp shape file, where each entry represents a unique geo-location point per site but often contains duplicates. However, this data cannot be used directly because the license status or mode of operation does not always correlate with the actual status of the well and often contains duplicates. Therefore, we work with domain experts to perform quality control as illustrated in Figure 2.

First, we remove duplicate entries from the well metadata, which often contain multiple instances of the same well identified by duplicate license numbers. We resolve these duplicates by retaining the most recent update. A similar approach is applied to the shapefile, where duplicates are resolved using the license date.

Table 2: Statistics of instances and wells across the dataset.

Split	Total Patches	Wells/ Non-Wells Patches	Count of Well Type in Wells Patches of Split		
			Abandoned	Suspended	Active
Train	167436	83718	46342	47595	100294
Validation	9463	4731	3166	2671	2406
Test	11789	5894	4024	3609	3340

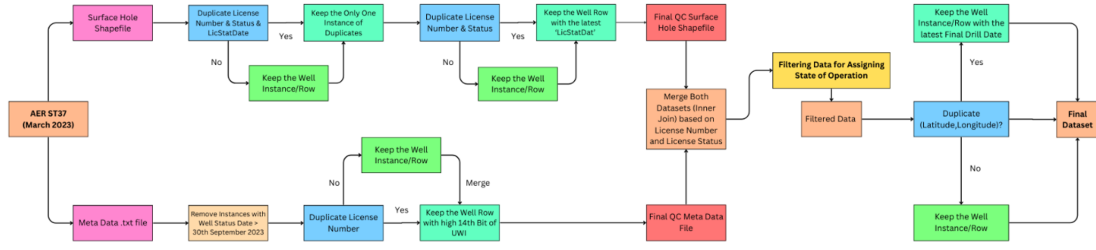


Figure 2: Flowchart depicting our process for AER ST37 dataset cleaning and quality control.

Afterward, we merge both datasets and filter the data, categorizing the wells as active, abandoned, or suspended based on criteria developed in consultation with domain experts, as shown in Table 3. We check for duplicate location coordinates in the dataset and resolve them by retaining the instance with the latest drill date.

Finally, we ensure all the well instances in the dataset are within Alberta’s boundaries. The raw metadata file has around 637,000 instances, while the surface hole geometry file has around 512,000 instances. After filtering and performing quality control on the datasets with domain experts, we have around 217,000 instances. We then calculate the geographical bounds covered by the well instances across the province and divide the region into non-overlapping square image patches, each covering an area of 1.1025 sq km (with sides of 1050m).

These images include various numbers of individual wells (see Fig. 1), and we ensure that an approximately equal number of patches exist with and without wells. As a result of this process, some samples were excluded due to being located outside Alberta’s geographical boundaries, leading to a final total of approximately 213,000 well instances in the dataset patches.

### 3.2 Dataset Splitting

To create a well-distributed dataset that represents various geographical regions and offers a diverse dataset for evaluation and testing, we developed a splitting algorithm (see Algorithm 1). Our splitting approach focuses on balancing regions, not individual examples, ensuring that both the training and test sets reflect a diverse range of regions from Alberta’s varied landscape. This approach preserves diversity and simulates real-world conditions where imbalances are common.

This method involves forming small clusters  $k_{1i}$  of nearby well patches based on their centroids as illustrated in Figure 3 (a). These small clusters are then grouped into larger, non-intersecting super-clusters  $k_{2i}$ , with each super-cluster representing a city or larger geographical area. The formation of super-clusters involves calculating a centroid for each  $k_{1i}$  cluster based on the centroids of the well patches it contains as illustrated in Figure 3 (b). By clustering wells in this manner, we ensure that  $k_{1i}$  clusters group wells from nearby localities together, while  $k_{2i}$  clusters group wells from the same geographic region as illustrated in Figure 3 (c). Thus, each  $k_{2i}$  cluster represents a geographic distribution, with each  $k_{1i}$  cluster within it representing a sample of that distribution.

To ensure a diverse and well-distributed evaluation and testing of our machine learning model, we select the  $k_{1i}$  clusters with the two fewest well instances from each  $k_{2i}$  super-cluster for inclusion in the evaluation and test sets. This approach ensures a diverse representation of the dataset as observed in Figure 3 (d).

Table 3: Information on the numbers of wells represented in the dataset across different states (suspended, abandoned, and active). It also includes domain-specific metadata, such as the mode of operation and the types of fossil fuels extracted, which were used for filtering and quality control.

Well State	Count	License Status	Mode Short Description	Fluid Short Description
Suspended	55007	Suspension	All	Gas, Crude oil, Crude bitumen, Liquid petroleum gas, Coalbed methane-coals and other Lith,
		Issued Amended	Suspended	
Abandoned	54947	Abandoned	All	Coalbed methane-coals only, Shale gas only, Acid gas, CBM and shale and other sources, Shale gas and other sources.
		Issued Amended	Abandoned, Abandoned Zone, Junked and Abandoned.	
Active	107139	Issued	Flowing, Pumping, Gas Lift.	
		Amended Re-Entered	Abandoned and Re-Entered	



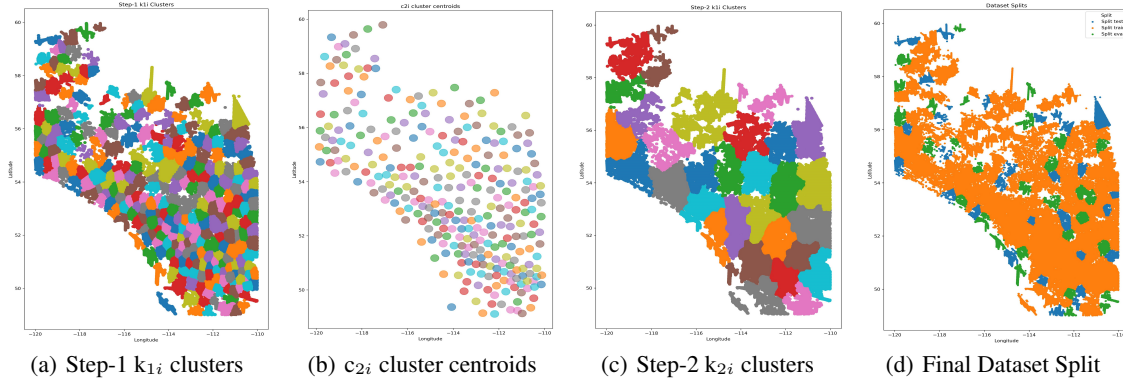


Figure 3: Illustration of the outcome of applying our dataset splitting algorithm: In Figures (a) to (c), different colors represent various cluster IDs. In Figure (d), blue refers to the training set, orange to the validation set, and green to the test set.

---

**Algorithm 1** Clustering Algorithm for Dataset Splitting

---

$W$ : Set of image patches ids containing wells ;  $NW$ : Set of image patches ids not containing wells

**Input:**  $x_i$  represents the  $i$ -th patch with centroid coordinates  $c_i$ , where  $i \in W$  or  $i \in NW$  ;

**Output:**  $T_s$ : Test Set ;  $T_r$ : Train Set ;  $E_v$ : Eval Set ;

**Step 1: Clustering into  $M$  Clusters**

Perform K-Means Clustering  $k_1(*)$  with  $M$  clusters using all centroid coordinates  $c_i$ , where  $i \in W$ .

Assign each  $i$ -th patch into the  $m$ -th cluster where  $m \in \{1, \dots, M\}$  and  $i \in W$ : cluster  $k_{1i} = k_1(c_i) = m$  and update patches  $(x_i, c_i, k_{1i})$

**for**  $z \in \{1, \dots, M\}$  **do**

$W_{cz} = \{j \in W \mid k_{1j} = z\}$

Calculate cluster centroids  $c_{2j}$  based on values of  $c_i$  and update patch:  $(x_i, c_i, k_{1i}, c_{2j})$ , where  $i \in W_{cz}$ .

**end for**

**Step 2: Clustering into  $N$  Super Clusters**

Let  $W_{cc}$  be the set of unique  $c_{2j}$  for  $j \in W$

Perform K-Means clustering  $k_2(*)$  with  $N$  clusters using all  $c_{2i} \in W_{cc}$ .

Assign each  $c_{2i} \in W_{cc}$  to  $n$ -th cluster, where  $n \in \{1, \dots, N\}$  &  $k_{2i} = k_2(c_{2i}) = n$ .

Update patches  $(x_j, c_j, k_{1j}, c_{2j}, k_{2j})$  where  $c_{2j} = c_{2i}$  and  $j \in W$ .

**Step 3: Assigning Patches to Sets**

**for**  $z \in \{1, \dots, N\}$  **do**

Find all  $j$  with  $k_{2j} = z$ , where  $j \in W$  as  $W_{fz}$ .

Find unique  $k_{1j}$  and count  $o_j$  associated with it for  $j$  in  $W_{fz}$ . The, assign  $k_{1j}$  with minimum counts as  $\min_1$  and  $\min_2$ .

For each  $i$  in  $W_{fz}$ , append  $i$  to  $E_v$  if  $k_{1i} = \min_1$ , to  $T_s$  if  $k_{1i} = \min_2$ , otherwise to  $T_r$ .

**end for**

**Step 4: Assigning Non-Well Patches**

**for** each set\_counter in  $\{E_v, T_s, T_r\}$  **do**

**for** each unique  $k_{1i}$  as  $z_i \in \text{set\_counter}$  **do**

Find convex hull radius  $r(z_i)$  of area occupied by  $c_j$ , where  $j \in \text{set\_counter}$  &  $k_{1j} = z_i$ .

Locate non-well patches  $f \in NW$  within radius  $r(z_i)$  not in any other cluster; Assign  $f$  to cluster  $z_i$ :  $(x_f, c_f, k_{1f})$  :

$k_{1f} = z_i$ .

**end for**

**end for**

**Step 5: Imbalance Correction**

$T_w$  refers to Count of Well Instances &  $T_{nw}$  refers to Count of Non-Well Instances in a Dataset Split

**if**  $T_{nw} > T_w$  **then**

Identify clusters  $k_{1j}$  in data split contributing to the imbalance of excess non-well patches, assign to  $W_{ic}$

**for** each  $i$  in  $W_{ic}$  **do**

$R(i) = (T_{nw} - T_w) \cdot \frac{\text{Count\_Non\_Wells}(k_{1i})}{\sum \text{Count\_Non\_Wells}(k_{1l}) \text{ where } l \in W_{ic}}$  ; where  $R(i)$  is the no. of Samples to be Removed from  $i$ -th Cluster.

**end for**

**else**

Sample non-well patches  $x_j$  :  $j \in NW$  &  $j \notin k_{1j}$ .

**end if**

---

Moreover, we maintain an equal distribution of well and non-well patches. In cases of imbalance in non-well images, we exclude such patches from the contributing  $k_{1i}$  clusters as specified in Algorithm 1. For imbalances in well images, we sample non-well patches that are not part of any other clusters.

The parameters used in constructing the dataset are  $M = 300$  and  $N = 30$ . These were picked heuristically so as to create a well-distributed dataset. Alberta’s varied landscape offers a rich environment for creating a comprehensive oil well dataset. Training machine learning models on this extensive dataset improves their robustness and ability to generalize to similar, less-studied regions, thereby supporting well detection and efforts to mitigate global warming. By forming non-overlapping clusters ( $k_{1i}$ ), each with its own well and non-well patches, we minimize the risk of data leakage while ensuring diversity. We also balanced non-well images across clusters to better simulate real-world conditions and maintain the diversity of the dataset.

### 3.3 Satellite Imagery Acquisition & Label Creation

We used PlanetScope-4-Band imagery [9] featuring RGB and Near Infrared bands to represent satellite images of the region with a medium resolution of about 3 meters per pixel. PlanetScope, a product of Planet Labs, consists of approximately 130 satellites that can image the entire Earth’s land surface daily, collecting up to 200 million sq. km of data each day. We obtained Surface Reflectance imagery, which is offset-corrected, flat-field-corrected, ortho-rectified, visually processed, and radio-metrically corrected. These processes ensure consistency across varying atmospheric conditions and minimize uncertainty in spectral response over time and location, making the data ideal for various applications. We choose Planet Labs data over other alternatives since it is updated daily, making it possible to pick a consistent time for all the images, which is important for training dataset consistency. It also provides multispectral imagery (4-band: RGB+Near Infrared), and the Near Infrared band is a useful addition (as we later verify in Table 6) since certain features, like ground depressions indicating well sites, may be more detectable in this band. Lastly, while other alternatives may be limited in remote regions, Planet’s global satellite constellation ensures more consistent coverage. All the imagery we use is made publicly available in the dataset. To ensure the highest quality, we selected images with no cloud cover. The images were acquired by Planet satellites within a timeframe that aligns with the well-location data from AER. We obtained satellite images for each sample based on geographical coordinates, ensuring an intersection between the actual area of interest and the acquired imagery.

We frame the task of identifying wells as both an object detection and segmentation task. In a real-world setting, high performance in either detection or segmentation would be sufficient for detection of wells; therefore we test both framings since it is not *a priori* clear which may be best suited to remote sensing algorithms. For each image patch, as shown in Figure 4, we generated corresponding segmentation maps and object detection annotations for all known wells in the image based on the point labels provided in the AER data.

For binary segmentation, we annotated each well site with a circle to match the teardrop shape typical for well sites. We standardized the diameter of a well site to a value of 90 meters (such sites typically range from 70 to 120 meters in diameter). We used the same scale to define bounding boxes in the object detection task, following the COCO [32] format for annotations. The overlap in ground truth bounding boxes for some of the wells in Figure 4 and Figure 9 reflects the clustering of multiple wells in densely developed oil and gas sites, where the spatial overlap of wells and infrastructure is common. (Note that this is a characteristic of the data, not a limitation of our quality control strategy.) Additionally, we created multi-class segmentation maps, where each class represents a different state of the well (active, suspended, or abandoned), and included this information in the object detection annotations. (We do not perform multi-class segmentation experiments here, but it is possible that future researchers may find this task useful.)

Identifying wells at 3m resolution seems like a very difficult task. That said, it’s important to consider that ML models may actually have the potential to surpass human performance in this particular task, for several reasons. First, identifying wells at a 3m resolution from satellite imagery is extremely challenging and requires significant patience by a human. Additionally, there are few human experts in this field, as well identification typically relies on existing databases or on-the-ground field studies rather than detailed satellite image analysis. Finally, certain features (such as depressions in the ground representing well sites) may be easier to pick out in the infrared channel, which humans are not accustomed to using, as compared with the RGB channels.

## 4 Experiments

We evaluate the performance of deep learning models for binary segmentation and object detection tasks. Our focus includes all oil and gas wells, regardless of their operational status, since they exhibit similar footprints and consistent features, making them detectable in satellite imagery.

We augment images by randomly resizing images to  $256 \times 256$ , ensuring all bounding boxes remain intact for object detection. We then apply horizontal and vertical flipping with a probability of 0.25 each, followed by normalization using channel-wise mean and standard deviation calculated from the training split of the dataset.

The hyperparameters we use in these various models represent standard performant settings and are not intended to represent the outcome of hyperparameter optimization.

#### 4.1 Binary Segmentation

We selected well-known baseline models for binary segmentation, encompassing the deep CNN-based approaches U-Net, PAN, and DeepLabV3+, as well as the Transformer-based architectures Segformer and UperNet.

U-Net [33] was chosen for its widespread use as a baseline, offering an effective encoder-decoder architecture for multi-scale feature extraction. PAN [34] improves multi-scale context with pyramid pooling and attention mechanisms. DeepLabV3+ [35] was selected for its popularity in remote sensing tasks with its Atrous Convolution and ASPP module for capturing contextual information at various scales. SegFormer [36] is a transformer-based architecture designed for semantic segmentation, utilizing self-attention mechanisms for capturing long-range dependencies. UperNet [37] combines UNet and PSPNet [38] architectures, featuring a UNet-like structure for multi-scale feature fusion and PSPNet’s pyramid pooling module integrated with a Swin Transformer [39] backbone for efficient multi-scale processing.

We train all CNN-based models using a ResNet50 backbone, a batch size of 128, and the BCELogits loss function. To fine-tune the model, a cosine annealing scheduler [40] is used, which adjusts the learning rate smoothly in a cyclical manner by gradually decreasing it. We also experimented with additional backbones with U-Net to evaluate the impact of backbones with larger receptive fields and attention mechanisms. This included ResNeXt50 [41], which enhances feature learning through grouped convolutions; SE-ResNet50 [42], which introduces channel-wise attention with Squeeze-and-Excitation blocks; and EfficientNetB6 [43], known for its balanced scaling.

In segmentation, the combination of UperNet’s contextual aggregation and the ConvNeXt backbone’s efficient representation enables precise segmentation, particularly valuable for remote sensing applications. For transformer-based models, while both Segformer and UperNet use a Dice loss function and a polynomial learning rate scheduler, Segformer utilizes a mit-b0-ade [36] backbone with a batch size of 128, while UperNet uses ConvNeXT (small and base) and Swin Transformer backbones with a batch size of 64. All models are optimized using AdamW for 50 epochs.

We evaluate the binary segmentation task with respect to IoU, Precision, Recall, and F1-Score. High Precision corresponds to reducing false positives, while high Recall corresponds to reducing false negatives. IoU measures the overlap between predicted and ground truth masks, offering further insight into segmentation accuracy. F1-Score, the harmonic mean of precision and recall, provides a balanced measure considering both false positives and false negatives.

#### 4.2 Object Detection

For binary object detection, we consider both single-stage, i.e., RetinaNet [44], FCOS and SSD, and two-stage CNN-based architectures, i.e. Faster R-CNN [45].

RetinaNet [44] is a one-stage architecture trained using focal loss, which helps to address class imbalance. It uses a Feature Pyramid Network (FPN) for multi-scale feature extraction and efficient object detection across different scales. Faster R-CNN [45] is a two-stage model recognized for its high accuracy. It employs a Region Proposal Network (RPN) for generating region proposals and a separate network for predicting class labels and refining bounding box coordinates. FCOS (Fully Convolutional One-Stage Object Detection) [46] directly predicts object locations and categories from feature maps, which is effective for small object detection. SSD (Single Shot MultiBox Detector) [47] uses multiple feature maps at different scales, enhancing its accuracy for small objects.

All object detection models are trained using a ResNet50 backbone, except for SSD Lite, which is trained with a MobileNet backbone. The batch size is set to 256 for Faster R-CNN and FCOS and 512 for RetinaNet and SSD Lite. We used a cosine annealing scheduler [40] and trained all models for 120 epochs. All models are optimized using the AdamW optimizer.

For binary object detection model evaluation, we calculate Intersection over Union (IoU) at various thresholds (e.g.,  $\text{IoU}_{0.1}$ ,  $\text{IoU}_{0.3}$ ,  $\text{IoU}_{0.5}$ ), which measures how well predicted bounding boxes align with ground truth. IoU is computed by dividing the area of overlap by the area of their union, with higher values indicating better alignment. IoU thresholds define the minimum overlap required for a predicted box to match a ground truth box. (For example, an  $\text{IoU}_{0.5}$  threshold means a predicted box must have at least 50% overlap with a ground truth box to be considered a correct detection.)

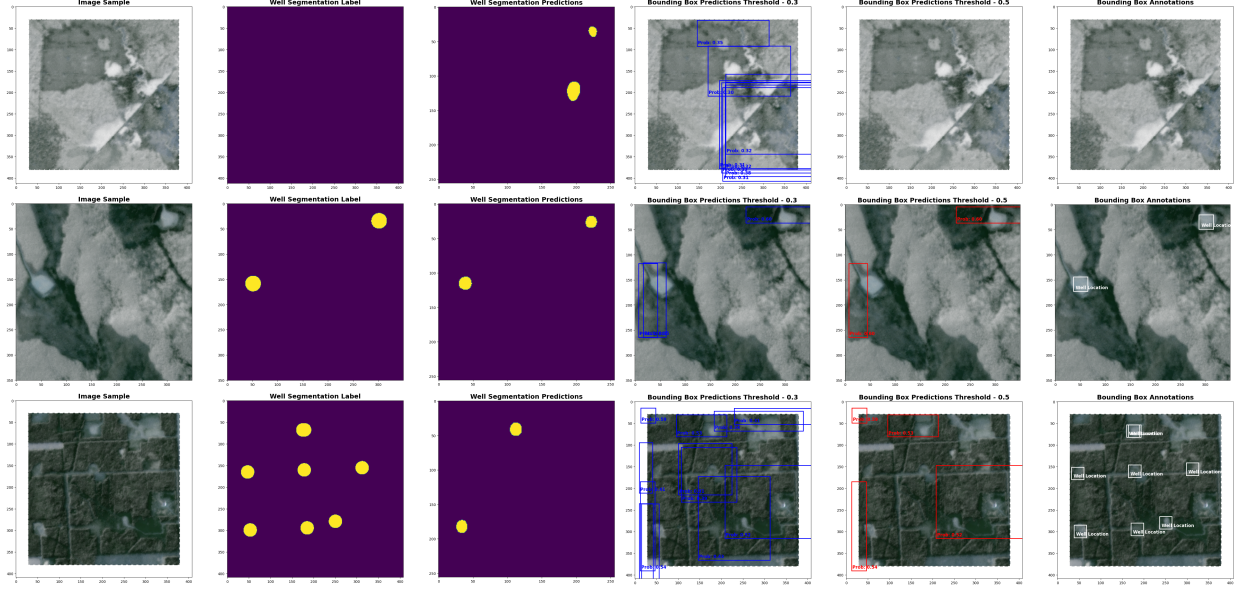


Figure 4: A sample image patch from our dataset includes examples with no wells, two wells, and multiple wells. Additionally, we present qualitative results with predictions generated by our Segmentation U-Net (EfficientNet-B6) and Detection FCOS model.

We also assess Mean Average Precision (mAP), including  $mAP_{50}$  and  $mAP_{50:95}$ , measuring the model’s precision-recall trade-off and detection accuracy at various IoU thresholds.  $mAP_{50}$  measures precision at an IoU threshold of 0.5, while  $mAP_{50:95}$  averages precision across IoU thresholds from 0.5 to 0.95. Higher mAP scores reflect better detection accuracy and precision. While higher IoU values indicate better accuracy for individual predictions, mAP provides a broader measure of detection performance by capturing precision across different IoU criteria.

## 5 Results

Our tasks involve identifying a roughly circular well region with a 90m diameter in real life, which translates to less than 30 pixels in satellite imagery due to resizing and other augmentations.

This poses a challenge for machine learning models given the heterogeneous nature of the background, including various similarly shaped and sized features of the natural and built environment. Additionally, vegetation can occlude wells in RGB channels, highlighting the importance of near-infrared imagery for guidance. The wells themselves also vary somewhat in shape and can be in various states of disrepair as a result of differing ages and maintenance.

### 5.1 Binary Segmentation

For the binary segmentation task framing, we train Models (from scratch) using both CNN-based and Transformer-based backbones, considering the prevalent imbalance in the image data due to the small size of wells. Although we did use 3-dimensional, ImageNet initialized weights of the backbone but modified the initial layers afterwards to support 4-dimensional multispectral images.

Among our models, as shown in Table 4, the traditional U-Net with EfficientNetB6 backbone performs the best, with CNN-based models showing the highest IOU of  $60.4 \pm 0.3$  and F1-Score of  $64.8 \pm 0.4$ . While a ResNet50-based backbone achieves the highest Precision of  $90.2 \pm 2.2$ , indicating more accurate predictions of well instances compared to other models. Precision, which reflects the accuracy of our positive detections compared to the ground truth, is crucial. However, a high recall value ensures the model captures most actual well instances, reducing the risk of missing important information. Thus, the Uper-Net model with the highest recall value of  $73.1 \pm 0.1$ , which excels at capturing global context information, appears a good candidate for this task, given a decent precision score.

Taking into account both precision and recall, U-Net with EfficientNetB6 backbone performs well, suggesting the utility of a larger backbone with a bigger receptive field. However, ConvNeXt Small provides a trade-off between

Table 4: Results for the binary segmentation task for a variety of models evaluated over the test set. We report the Intersection over Union (IoU), precision, recall, and F1-score.

Architecture	Backbone	Params	GFLOPs	IoU	F1 Score	Precision	Recall
U-Net	ResNet50	32.52M	21.42	58±0.5	61.9±0.8	<b>90.2±2.2</b>	62.3±1.6
	ResNext50	32M	21.81	58.2±0.2	62.1±0.3	88.2±3.5	63.6±1.7
	SE_ResNet50	35.06M	20.83	58.9±0.7	62.9±0.7	88.8±1.6	64.4±1.4
	EfficientNetB6	43.83M	-	<b>60.4±0.3</b>	<b>64.8±0.4</b>	87.8±0.4	66.3±0.3
PAN	ResNet50	24.26M	17.47	57.8±0.8	61.5±0.9	89.3±1.2	61.5±0.9
DeepLabV3+	ResNet50	26.68M	18.44	56.8±0.7	60.6±0.7	89.4±1.3	61.8±1.1
Segformer	mit-b0-ade	3.72M	3.52	57.6±0.5	61.3±0.6	82.6±2.9	69.2±2.1
	ConvNexT-Small	128.29M	81.76	59.4±0.1	63.5±0.1	81.5±0.5	71.5±0.4
UperNet	ConvNexT-Base	146.27M	121.99	59.7±0.3	63.8±0.2	81.1±0.7	72.2±0.2
	swin small	81.15M	134.20	59.9±0.7	64.2±0.7	80.6±0.5	<b>73.1±0.1</b>

computational efficiency and performance, requiring fewer GFLOPs and parameters compared to UperNet with Swin Small while achieving similar performance.

## 5.2 Binary Object Detection

Our evaluation, as shown in Table 5, indicates that while all models perform reasonably well in terms of aligning predicted and actual well locations, performance in the object detection task is overall lower than for segmentation – indicating that potentially segmentation is simply a better framing for this task in real-world settings.

The observed gap in performance is likely due to the small size of the wells. It is well-known that single-stage CNN architectures (such as FCOS and SSD) often demonstrate better performance on small object detection than two-stage methods (such as Faster R-CNN), and this aligns with our observations. The exception here is the single-stage method RetinaNet, which, although it has comparable IoU scores, struggles to detect wells accurately.

SSD Lite stands out with the highest  $\text{IoU}_{0.5}$  score of  $65.07 \pm 0.03$  and  $\text{IoU}_{0.3}$  score of  $50.3 \pm 0.08$ . Whereas all models are quite similar in terms of  $\text{IoU}_{0.1}$ , the highest score by FasterRCNN is  $36.79 \pm 1.07$ . Thus, SSD Lite and FCOS excel in localization, especially at higher IoU thresholds, while Faster R-CNN is adept at detecting objects with minimal overlap. All models demonstrate low performance in terms of  $\text{mAP}_{50}$ , which assesses precision-recall trade-off and detection accuracy at an IoU threshold of 0.5. FCOS achieves the of  $9.67 \pm 1.47$  while SSD Lite achieves a score of  $9.76 \pm 0.39$ . This may be due to these models not producing region proposals confidently enough, especially in instances with a large number of wells. Whereas over a broader evaluation with  $\text{mAP}_{50:95}$  which averages precision across IoU thresholds from 0.5 to 0.95. All models apart from RetinaNet provide much better results, with FCOS achieving the highest score of  $30.46 \pm 3.11$ , indicating a decent performance in the identification of well instances. While IoU scores are decent with increasing thresholds, the mAP scores indicate that a more complex model may be required for this task.

## 5.3 Value Added from Dataset Breadth

In these experiments, we consider the value provided by our inclusion of (i) near-infrared (NIR) imagery in addition to RGB channels, and (ii) the inclusion of abandoned and suspended wells in addition to active wells.

Table 5: Results for the object detection task for a variety of models evaluated over the test set. We report the intersection over union (IoU) over thresholds 0.1, 0.3, 0.5 and the mean average precision (mAP) for both  $\text{IoU} = 0.5$  and  $\text{IoU} \in [0.5, 0.95]$  thresholds.

Architecture	Backbone	Params	GFLOPs	$\text{IoU}_{0.1}$	$\text{IoU}_{0.3}$	$\text{IoU}_{0.5}$	$\text{mAP}_{50}$	$\text{mAP}_{50:95}$
RetinaNet		18.87M	0.93	24.58±0.11	43.07±0.8	59.79±0.36	0.18±0.28	0.72±1.12
FasterRCNN	ResNet50	41.09M	24.7	<b>36.79±1.07</b>	46.95±0.66	61.29±0.35	5.20±1.00	19.12±3.41
FCOS		31.85M	25.81	34.79±0.99	48.51±0.59	62.66±0.43	<b>9.67±1.47</b>	<b>30.46±3.11</b>
SSD Lite	MobileNet	3.71M	0.64	33.91±0.18	<b>50.30±0.08</b>	<b>65.07±0.03</b>	<b>9.76±0.39</b>	25.14±0.66

Table 6: Results for the binary segmentation task for U-Net with ResNet50 backbone, trained with and without NIR imagery. We find that NIR significantly improves performance.

Modality	IoU	F1 Score	Precision	Recall
RGB+NIR	<b>58.00±0.50</b>	<b>61.9±0.80</b>	<b>90.20±2.20</b>	<b>62.30±1.60</b>
RGB	56.60±0.44	60.50±0.35	87.00±1.40	<b>62.54±0.13</b>

Table 7: Results for object detection task for the FCOS Model with ResNet50 backbone evaluated over the test set for multiple input modality. We report the intersection over union (IoU) over thresholds 0.1, 0.3, 0.5 and the mean average precision (mAP) for both IoU= 0.5 and IoU∈ [0.5, 0.95] thresholds.

Modality	IoU <sub>0.1</sub>	IoU <sub>0.3</sub>	IoU <sub>0.5</sub>	mAP <sub>50</sub>	mAP <sub>50:95</sub>
RGB+NIR	<b>34.79±0.99</b>	<b>48.51±0.59</b>	<b>62.66±0.43</b>	<b>9.67±1.47</b>	<b>30.46±3.11</b>
RGB	32.39±2.88	46.80±2.07	61.23±1.58	5.7±3.65	20.00±10.40

### 5.3.1 Benefits of NIR imagery: (RGB v/s RGB+NIR)

We find that including the NIR band significantly enhances both object detection and segmentation performance compared to purely RGB data. In object detection (Table 7), RGB+NIR achieves higher Intersection over Union (IoU) scores across all thresholds (0.1, 0.3, and 0.5) and a considerable increase in mAP@50 (9.67±1.47 vs. 5.7±3.65) and mAP@50:95 (30.46±3.11 vs. 20±10.4). Similarly, in segmentation (Table 6), RGB+NIR shows superior performance in IoU (58±0.5 vs. 56.6±0.44), F1 Score (61.9±0.8 vs. 60.5±0.35), and Precision (90.2±2.2 vs. 87±1.4), while maintaining a slightly lower Recall (62.3±1.6 vs. 62.54±0.13). These improvements are due to the enhanced spectral information, which is particularly effective in identifying features such as ground depressions, often more visible in the NIR band.

### 5.3.2 Benefits of Using Multiple Well Types.

While much past work has focused on active wells, we show that training on such data is insufficient to detect abandoned and suspended wells (which are often significantly harder to e.g. degradation and vegetation growth over time). The results in Table 8 emphasize the necessity of including all well types (active, suspended, and abandoned) in the training dataset to ensure comprehensive detection across diverse scenarios. While training exclusively on active wells achieves high performance for individual well types, but it significantly under-performs in mixed-type contexts (IoU: 0.502), indicating poor generalization when all well types are present. Training exclusively on active wells significantly under-performs in mixed-type contexts (IoU: 0.502), indicating poor generalization when all well types are present. Conversely, training on all well types improves the model’s ability to handle real-world heterogeneity, as reflected by a higher IoU (0.576), F1 score (0.614), and recall (0.614) for the test set. The enhanced recall demonstrates the model’s capability to identify a broader range of wells, crucial for environmental monitoring, where missing even a single abandoned well could result in unaddressed methane emissions or groundwater contamination. Precision for active-only training (0.998) is higher than the model trained on all well types (0.913), but its inability to detect all wells in an image (due to low recall) limits its applicability. Therefore, incorporating all well types in training ensures balanced, reliable performance, allowing for accurate detection and classification in diverse and realistic contexts.

Table 8: Performance comparison of U-Net with ResNet50 backbone for binary segmentation trained on active wells only versus all well types. Our results demonstrate that training merely on active wells is not sufficient to detect abandoned and suspended wells in practice – highlighting the importance of including all three types in the dataset.

Metric	Train Set (Well Type Label Present)	Test Set
IoU	Active (I)	0.502
	All (I+II+III)	<b>0.576</b>
F1 Score	Active (I)	0.503
	All (I+II+III)	<b>0.614</b>
Precision	Active (I)	<b>0.998</b>
	All (I+II+III)	0.913
Recall	Active (I)	0.502
	All (I+II+III)	<b>0.614</b>

## 6 Limitations

We do not envision any significant negative uses of our work. Localization of wells is primarily of interest to the climate change mitigation community and is not, for example, a primary means whereby fossil fuel companies select new locations for drilling. Therefore, we do not believe this dataset is susceptible to dual use risks.

One potential limitation of our work is that we rely on well locations listed by the Alberta Energy Regulator. It is likely that some true well locations are missing in this data, leading to the potential for false negatives in the ground-truth data for this problem. However, it is to be expected that this will not significantly affect the training of algorithms since these labels represent a small fraction of the negative locations in the dataset, and deep learning algorithms are known to be robust to moderate amounts of label noise (see e.g. [48]). Instead the effect may simply be that the reported test accuracy is actually lower than the true value (due to certain correctly predicted well locations being evaluated as false). We hope to investigate such effects further in future work.

Our dataset is focused on Alberta, because (1) it is a very large region with a significant amount of high-quality labeled data available, (2) it is one of the world’s most important locations for oil and gas production, so identifying wells in Alberta is of immediate impact. Future works may wish to assess the capacity for few- or zero-shot transfer learning from Alberta to other regions with a high expected concentration of abandoned wells, including the Appalachian and Mountain West regions of the United States, as well as a number of former Soviet states.

## 7 Conclusion

In this paper, we present the first large-scale benchmark dataset aimed at identifying oil and gas wells, with a focus on abandoned and suspended wells, which are a significant source of greenhouse gases and other pollutants.

We combine high-resolution imagery, an extensive database of well locations, and expert verification to create the Alberta Wells Dataset. We frame well identification both in terms of object detection and binary segmentation and evaluate the performance of a wide range of popular deep learning methods on these tasks. We find that the UperNet Model (with a ConvNext backbone), in particular, represents the most promising baseline for the binary segmentation task, while for object detection, all models demonstrate more mixed results, with Single Stage Models (such as FCOS and SSD) providing a relatively promising baseline. These results show that the Alberta Wells Dataset represents both a challenging as well as a societally impactful set of tasks.

The value added by the dataset is twofold. First, most global fossil fuel-producing regions do not have databases of well locations comparable to that provided by AER. Alberta’s varied landscape provides an ideal setting for developing algorithms for the detection of wells, which can then be used directly in other locations or fine-tuned. Second, even in Alberta, the list developed by AER is not comprehensive, and many abandoned wells are believed to be missing; remote sensing algorithms can provide candidate locations for domain experts to examine so as to determine the true number and locations of abandoned wells in Alberta. Overall, we hope that our work will make it possible to (i) better estimate the total effects of well-related methane emissions (currently extremely uncertain [1]) and groundwater contamination, (ii) prioritize wells to be plugged and decontaminated. We believe that the scalability of remote sensing will make it an invaluable tool in mitigating the global environmental impact of abandoned oil and gas wells.

## 8 Acknowledgments and Disclosure of Funding

This research was made possible by the generous access to the Planet Lab subscription provided by Dr. Tim Elrick from McGill University’s Geography Department. We acknowledge the essential support from Planet Labs for their academic subscription and guidance on the public release of datasets. The Alberta Energy Regulator’s AER ST37 dataset was a crucial resource for our work.

The authors are also grateful to Mila and the Digital Research Alliance of Canada for the vital computing facilities, and to NVIDIA Corporation for their indispensable computational resources. Special thanks to Francis Pelletier, the lab’s Data Engineer, whose crucial feedback on our data collection pipeline and coding significantly improved our methods.

## 9 Impact Statement

This work presents the first large-scale machine learning benchmark for pinpointing onshore oil and gas wells, including abandoned, suspended, and active wells. Our dataset, the Alberta Wells Dataset, contains over 200,000 well instances and high-resolution satellite imagery, enabling advancements in the identification of oil and gas wells. By framing the

problem as one of object detection and binary segmentation, we hope this dataset will help improve the scalability and accuracy of well detection techniques.

Abandoned wells, particularly those that leak methane and other pollutants, pose a major environmental challenge. By improving methods for detecting these wells, this work aims to reduce their environmental impact by identifying high-emission sites that can be prioritized for remediation. This can contribute to mitigating climate change by helping to reduce harmful emissions from these otherwise difficult-to-detect sources.

To enable wider responsible uses of the dataset, we will release it under a non-commercial usage license, making it available for academic and research purposes only. We do not foresee significant negative impacts arising from this work. Dual uses of the algorithms we outline here are limited, and the algorithms used are comparatively small-scale and have low energy and carbon footprint.

By improving detection techniques and providing access to valuable data, this work has the potential to support global efforts in identifying and addressing abandoned oil and gas wells, ultimately contributing to environmental sustainability and climate action.

## References

- [1] James P Williams, Amara Regehr, and Mary Kang. Methane emissions from abandoned oil and gas wells in Canada and the United States. *Environmental science & technology*, 55(1):563–570, 2020.
- [2] ECCC. Greenhouse gas emissions. <https://www.canada.ca/en/environment-climate-change/services/environmental-indicators/greenhouse-gas-emissions.html>, 2024. [Accessed 28-09-2024].
- [3] Aaron G Cahill, Roger Beckie, Bethany Ladd, Elyse Sandl, Maximillian Goetz, Jessie Chao, Julia Soares, Cara Manning, Chitra Chopra, Niko Finke, et al. Advancing knowledge of gas migration and fugitive gas from energy wells in northeast british columbia, canada. *Greenhouse Gases: Science and Technology*, 9(2):134–151, 2019.
- [4] Stuart N Riddick, Mercy Mbua, Arthur Santos, Ethan W Emerson, Fancy Cheptonui, Cade Houlihan, Anna L Hodshire, Abhinav Anand, Wendy Hartzell, and Daniel J Zimmerle. Methane emissions from abandoned oil and gas wells in colorado. *Science of The Total Environment*, 922:170990, 2024.
- [5] Mary Kang, Shanna Christian, Michael A Celia, Denise L Mauzerall, Markus Bill, Alana R Miller, Yuheng Chen, Mark E Conrad, Thomas H Darrah, and Robert B Jackson. Identification and characterization of high methane-emitting abandoned oil and gas wells. *Proceedings of the National Academy of Sciences*, 113(48):13636–13641, 2016.
- [6] Esther Rolf, Konstantin Klemmer, Caleb Robinson, and Hannah Kerner. Mission critical – satellite data is a distinct modality in machine learning. In *International Conference in Machine Learning (ICML)*, 2024.
- [7] Jun Yang, Peng Gong, Rong Fu, Minghua Zhang, Jing Chen, Shunlin Liang, Bing Xu, Jiancheng Shi, and Robert Dickinson. The role of satellite remote sensing in climate change studies. *Nature Climate Change*, 3:875–883, 09 2013.
- [8] Hao Sheng, Jeremy A. Irvin, Sasankh Munukutla, Shenmin Zhang, Christopher Cross, Kyle T. Story, Rose Rustowicz, Cooper W. Elsworth, Zutao Yang, Mark Omara, Ritesh Gautam, Robert B. Jackson, and A. Ng. OGNet: Towards a global oil and gas infrastructure database using deep learning on remotely sensed imagery. *ArXiv*, abs/2011.07227, 2020.
- [9] Planet Labs PBC. Planet application program interface: In space for life on earth. <https://api.planet.com>, 2024.
- [10] Gencer Sumbul, Marcela Charfuelan, Begüm Demir, and Volker Markl. BigEarthNet: A large-scale benchmark archive for remote sensing image understanding. *IGARSS 2019 - 2019 IEEE International Geoscience and Remote Sensing Symposium*, pages 5901–5904, 2019.
- [11] Dimitrios Sykas, Maria Sdraka, Dimitrios Zografakis, and Ioannis Papoutsis. A Sentinel-2 multi-year, multi-country benchmark dataset for crop classification and segmentation with deep learning. *IEEE Journal of Selected Topics in Applied Earth Observations and Remote Sensing*, 2022.
- [12] Gabriel Tseng, Ivan Zvonkov, Catherine Lilian Nakalembe, and Hannah Kerner. CropHarvest: A global dataset for crop-type classification. In *Conference on Neural Information Processing Systems (NeurIPS) Datasets and Benchmarks Track*, 2021.
- [13] Mélisande Teng, Amna Elmustafa, Benjamin Akera, Yoshua Bengio, Hager Radi, Hugo Larochelle, and David Rolnick. Satbird: a dataset for bird species distribution modeling using remote sensing and citizen science data. In *Advances in Neural Information Processing Systems (NeurIPS)*, 2023.



- [14] Nikolaos Ioannis Bountos, Arthur Ouaknine, and David Rolnick. FoMo-Bench: a multi-modal, multi-scale and multi-task Forest Monitoring Benchmark for remote sensing foundation models. *arXiv e-prints*, page arXiv:2312.10114, December 2023.
- [15] Adam Van Etten, Daniel Hogan, Jesus Martinez-Manso, Jacob Shermeyer, Nicholas Weir, and Ryan Lewis. The multi-temporal urban development spacenet dataset, 2021.
- [16] Xiaodao Chen, Dongmei Zhang, Yuewei Wang, Lizhe Wang, Albert Y. Zomaya, and Shiyan Hu. Offshore oil spill monitoring and detection: Improving risk management for offshore petroleum cyber-physical systems. *2017 IEEE/ACM International Conference on Computer-Aided Design (ICCAD)*, pages 841–846, 2017.
- [17] Yuewei Wang, Xiaodao Chen, and Lizhe Wang. Cyber-physical oil spill monitoring and detection for offshore petroleum risk management service. *Scientific Reports*, 13, 2023.
- [18] Junfang Yang, Yi Ma, Yabin Hu, Zongchen Jiang, J. Zhang, Jianhua Wan, and Zhongwei Li. Decision fusion of deep learning and shallow learning for marine oil spill detection. *Remote. Sens.*, 14:666, 2022.
- [19] Samyak Prajapati, Amrit Raj, Yash Chaudhari, Akhilesh Nandwal, and Japman Singh Monga. OGInfra: Geolocating oil & gas infrastructure using remote sensing based active fire data. *ArXiv*, abs/2210.16924, 2022.
- [20] Bryan Zhu, Nicholas Lui, Jeremy Irvin, Jimmy Le, Sahil Tadwalkar, Chenghao Wang, Zutao Ouyang, Frankie Y. Liu, Andrew Y. Ng, and Robert B. Jackson. METER-ML: A multi-sensor Earth observation benchmark for automated methane source mapping, 2022.
- [21] Mark Omara, Ritesh Gautam, Madeleine A. O’Brien, Anthony Himmelberger, Alexandre Puglisi Barbosa Franco, Kelsey Meisenhelder, Grace Hauser, David R. Lyon, Apisada Chulakadabba, C. Chan Miller, Jonathan E. Franklin, Steven C. Wofsy, and Steven P. Hamburg. Developing a spatially explicit global oil and gas infrastructure database for characterizing methane emission sources at high resolution. *Earth System Science Data*, 2023.
- [22] Huan Chang, Lu Bai, Zhibao Wang, Mei Wang, Ying Zhang, Jinhua Tao, and Liangfu Chen. Detection of over-ground petroleum and gas pipelines from optical remote sensing images. In *Remote Sensing*, 2023.
- [23] Zhibao Wang, Xi Zhao, Lu Bai, Mei Wang, Man Zhao, Meng Fan, Jinhua Tao, and Liangfu Chen. Detection of heavy-polluting enterprises from optical satellite remote sensing images. In *IGARSS 2023 - 2023 IEEE International Geoscience and Remote Sensing Symposium*, pages 6474–6477, 2023.
- [24] Zhibao Wang, Lu Bai, Guangfu Song, Jie Zhang, Jinhua Tao, Maurice D. Mulvenna, Raymond R. Bond, and Liangfu Chen. An oil well dataset derived from satellite-based remote sensing. *Remote Sensing*, 13(6), 2021.
- [25] Yu Zhang, Lu Bai, Zhibao Wang, Meng Fan, Anna Jurek-Loughrey, Yuqi Zhang, Ying Zhang, Man Zhao, and Liangfu Chen. Oil well detection under occlusion in remote sensing images using the improved YOLOv5 model. *Remote Sensing*, 15(24), 2023.
- [26] Pengfei Shi, Qigang Jiang, Chao Shi, Jing Xi, Guo Tao, Sen Zhang, Zhenchao Zhang, B. Liu, Xin Gao, and Qian Wu. Oil well detection via large-scale and high-resolution remote sensing images based on improved YOLO v4. *Remote. Sens.*, 13:3243, 2021.
- [27] Jade Eva Guisiano, Éric Moulines, Thomas Lauvaux, and Jérémie Sublime. Oil and gas automatic infrastructure mapping: Leveraging high-resolution satellite imagery through fine-tuning of object detection models. In Biao Luo, Long Cheng, Zheng-Guang Wu, Hongyi Li, and Chaojie Li, editors, *Neural Information Processing*, pages 442–458, Singapore, 2024. Springer Nature Singapore.
- [28] Neel Ramachandran, Jeremy Irvin, Mark Omara, Ritesh Gautam, Kelsey Meisenhelder, Erfan Rostami, Hao Sheng, Andrew Y Ng, and Robert B Jackson. Deep learning for detecting and characterizing oil and gas well pads in satellite imagery. *Nature Communications*, 15(1):7036, 2024.
- [29] Hao Wu, Hongli Dong, Zhibao Wang, Lu Bai, Fengcai Huo, Jinhua Tao, and Liangfu Chen. Semantic segmentation of oil well sites using Sentinel-2 imagery. In *IGARSS 2023 - 2023 IEEE International Geoscience and Remote Sensing Symposium*, pages 6901–6904, 2023.
- [30] Hao Wu, Hongli Dong, Zhibao Wang, Lu Bai, Fengcai Huo, Jinhua Tao, and Liangfu Chen. Spatial information extraction of oil well sites based on medium-resolution satellite imagery. In *Image and Signal Processing for Remote Sensing XXIX*, volume 12733, page 127330K. International Society for Optics and Photonics, SPIE, 2023.
- [31] Alberta Energy Regulator AER. ST37 — aer.ca. <https://www.aer.ca/providing-information/data-and-reports/statistical-reports/st37>, 2024. [Accessed 06-06-2024].
- [32] Tsung-Yi Lin, Michael Maire, Serge J. Belongie, James Hays, Pietro Perona, Deva Ramanan, Piotr Dollár, and C. Lawrence Zitnick. Microsoft COCO: Common objects in context. In *European Conference on Computer Vision*, 2014.

- [33] Olaf Ronneberger, Philipp Fischer, and Thomas Brox. U-net: Convolutional networks for biomedical image segmentation. *ArXiv*, abs/1505.04597, 2015.
- [34] Hanchao Li, Pengfei Xiong, Jie An, and Lingxue Wang. Pyramid attention network for semantic segmentation. *ArXiv*, abs/1805.10180, 2018.
- [35] Liang-Chieh Chen, Yukun Zhu, George Papandreou, Florian Schroff, and Hartwig Adam. Encoder-decoder with atrous separable convolution for semantic image segmentation. In *European Conference on Computer Vision*, 2018.
- [36] Enze Xie, Wenhai Wang, Zhiding Yu, Anima Anandkumar, José Manuel Álvarez, and Ping Luo. Segformer: Simple and efficient design for semantic segmentation with transformers. In *Neural Information Processing Systems*, 2021.
- [37] Tete Xiao, Yingcheng Liu, Bolei Zhou, Yuning Jiang, and Jian Sun. Unified perceptual parsing for scene understanding. *ArXiv*, abs/1807.10221, 2018.
- [38] Hengshuang Zhao, Jianping Shi, Xiaojuan Qi, Xiaogang Wang, and Jiaya Jia. Pyramid scene parsing network. *2017 IEEE Conference on Computer Vision and Pattern Recognition (CVPR)*, pages 6230–6239, 2016.
- [39] Ze Liu, Yutong Lin, Yue Cao, Han Hu, Yixuan Wei, Zheng Zhang, Stephen Lin, and Baining Guo. Swin transformer: Hierarchical vision transformer using shifted windows. *2021 IEEE/CVF International Conference on Computer Vision (ICCV)*, pages 9992–10002, 2021.
- [40] Ilya Loshchilov and Frank Hutter. SGDR: Stochastic gradient descent with warm restarts. *arXiv: Learning*, 2016.
- [41] Saining Xie, Ross B. Girshick, Piotr Dollár, Zhuowen Tu, and Kaiming He. Aggregated residual transformations for deep neural networks. *2017 IEEE Conference on Computer Vision and Pattern Recognition (CVPR)*, pages 5987–5995, 2016.
- [42] Jie Hu, Li Shen, Samuel Albanie, Gang Sun, and Enhua Wu. Squeeze-and-excitation networks. *2018 IEEE/CVF Conference on Computer Vision and Pattern Recognition*, pages 7132–7141, 2017.
- [43] Mingxing Tan and Quoc V. Le. Efficientnet: Rethinking model scaling for convolutional neural networks. *ArXiv*, abs/1905.11946, 2019.
- [44] Tsung-Yi Lin, Priya Goyal, Ross B. Girshick, Kaiming He, and Piotr Dollár. Focal loss for dense object detection. *IEEE Transactions on Pattern Analysis and Machine Intelligence*, 42:318–327, 2017.
- [45] Shaoqing Ren, Kaiming He, Ross B. Girshick, and Jian Sun. Faster r-cnn: Towards real-time object detection with region proposal networks. *IEEE Transactions on Pattern Analysis and Machine Intelligence*, 39:1137–1149, 2015.
- [46] Zhi Tian, Chunhua Shen, Hao Chen, and Tong He. Fcos: Fully convolutional one-stage object detection. *2019 IEEE/CVF International Conference on Computer Vision (ICCV)*, pages 9626–9635, 2019.
- [47] W. Liu, Dragomir Anguelov, D. Erhan, Christian Szegedy, Scott E. Reed, Cheng-Yang Fu, and Alexander C. Berg. Ssd: Single shot multibox detector. In *European Conference on Computer Vision*, 2015.
- [48] David Rolnick, Andreas Veit, Serge Belongie, and Nir Shavit. Deep learning is robust to massive label noise. *arXiv preprint arXiv:1705.10694*, 2017.

## A Data Licensing

The AWD Dataset is released under a Creative Commons Attribution-NonCommercial 4.0 International (CC BY-NC 4.0) License (<https://creativecommons.org/licenses/by-nc/4.0/>). The satellite imagery for this project was acquired through Planet Labs' [9] Education & Research license, which allows the use of the data in publications and the creation of derivative products related to those publications. However, the raw imagery cannot be shared publicly. To adhere to these guidelines, we provide the data in HDF5 format, with the satellite imagery pre-processed to produce a derived product represented as a numpy array from Raster Vector. This process removes all geographic metadata.

This data is for academic use only and should not be used commercially. Proper credit to the current authors, Planet Labs [9], and the Alberta Energy Regulator [31] is required when using this data.

## B Dataset Information

The purpose of this dataset is to assist in training deep learning systems to identify oil and gas wells, including abandoned, suspended, and active ones. This will enable the detection of wells in a specific area, allowing comparison with government records. If discrepancies are found, experts can conduct further investigations, which can possibly lead to the discovery of an abandoned or suspended device that might not be present in government records.

### B.1 Dataset Structure

We provide training, validation, and testing sets, split using our proposed algorithm (as described in Section 3.2 of the main paper) to create a well-distributed dataset. The proposed method aims to create smaller regions of well concentration by clustering the centroids of patches. These regions are designed to be (a) mutually non-intersecting, (b) part of a larger geographic region by clustering the centroids of the initial clusters, and (c) containing a similar distribution of non-well patches within the same region.

This approach ensures that the training, validation, and test sets include representations from all geographic regions, providing a diverse and comprehensive evaluation. Thus, the dataset represents various geographical regions and offers a diverse benchmark for evaluation and testing.

Each dataset split is saved in an HDF5 format file, structured as described in the following sections, and then compressed into a .tar.gz file for faster transfer. Details on the number of samples in each set and the size of the dataset, both original and compressed, are presented in Table 3.

### B.2 Dataset File Directory Structure

The following directory structure is used for each dataset file being stored in a Hierarchical Data Format 5 (HDF5) file:

```
<Train/Test/Val>Set.h5
|---image
|   |---<sample_name>
|       |---Satellite Image (Multispectral Rasterio Image Data)
|       |---Meta Data of <sample_name>
|---label
|   |---binary_seg_maps
|       |---<sample_name>
|           |---Binary Segmentation Map (Rasterio Image Data)
|   |---multi_class_seg_maps
|       |---<sample_name>
|           |---Multiclass Segmentation Map (Rasterio Image Data)
|   |---bounding_box_annotations
|       |---<sample_name>
|           |---Bounding Box JSON Data (COCO Format)
|---author: Anonymous Author(s)
|---description: Alberta Wells Dataset: Pinpointing Oil and Gas Wells
                  from Satellite Imagery
```

Table 9: Dataset statistics represented across the various splits of the dataset.

Dataset Split	No of Samples	No of Wells in Split	Original HDF5 File Size (in Gb)	Compressed .tar.gz File Size (in Gb)
Train	167436	194231	322	100
Validation	9463	8243	19	5.7
Test	11789	10973	24	7.1
Total	188688	213447	365	112.8

### B.3 Structure of Dataset Directory

To enhance the efficiency of the data loader, we split the larger .h5 dataset into smaller .h5 files, each corresponding to a unique sample (image patch). By splitting the dataset in such a manner, we are able to improve the speed per iteration of the dataloader by over 100%. This results in the following data structure:

```
<Sample_Id>.h5
|---image
|   |---Satellite Image (Multispectral Rasterio Image Data)
|   |---Meta Data
|---label
|   |---binary_seg_maps
|       |---Binary Segmentation Map (Rasterio Image Data)
|   |---multi_class_seg_maps
|       |---Multiclass Segmentation Map (Rasterio Image Data)
|   |---bounding_box_annotations
|       |---Bounding Box JSON Data (COCO Format)
|---author: Anonymous Author(s)
|---description: Alberta Wells Dataset: Pinpointing Oil and Gas Wells
                  from Satellite Imagery
```

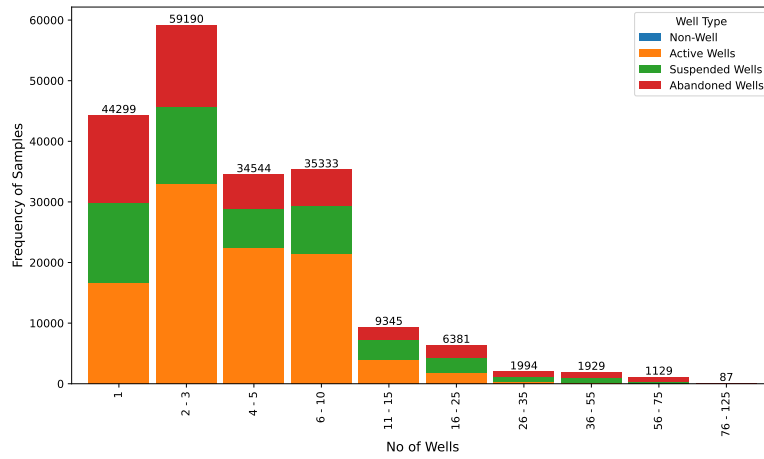
### B.4 Dataset Size & Distribution of Samples

Our dataset comprises over 94,000 patches of satellite imagery containing wells, with a total of 188,000 patches sourced from Planet Labs [9], covering more than 213,000 individual wells. Details about the distribution of the number of patches, wells present, and dataset split sizes are provided in Table 9, with the distribution of the number of wells per sample being described in Table 10. We also include an equal number of images that contain no wells in each dataset split. The distribution of wells per sample, along with the corresponding number of wells and the breakdown of well types, is illustrated in Figure 5 and detailed in Tables 11, 12, and 13. The geographic distribution of wells in the dataset can be visualized in Figure 6.

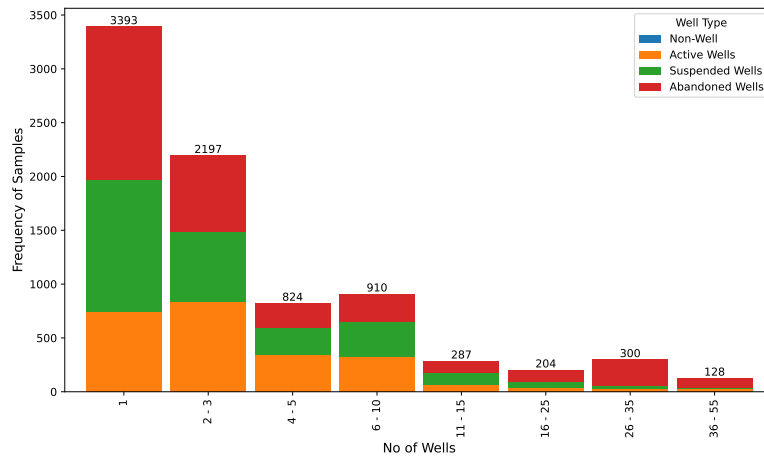
Table 10: The distribution of individual wells in positive samples from the dataset. We also include an equal number of images that contain no wells in each dataset split.

No of Wells in a Sample	Frequency of Well Instances in a Sample		
	Training Split	Validation Split	Test Split
1	44299	3393	4128
2 - 3	25378	979	1242
4 - 5	7899	190	328
6 - 10	4927	123	227
11 - 15	751	23	38
16 - 25	333	11	19
26 - 35	67	10	2
36 - 55	45	3	0
56 - 75	18	0	0
76 - 125	1	0	0
Total	83718	4732	5984

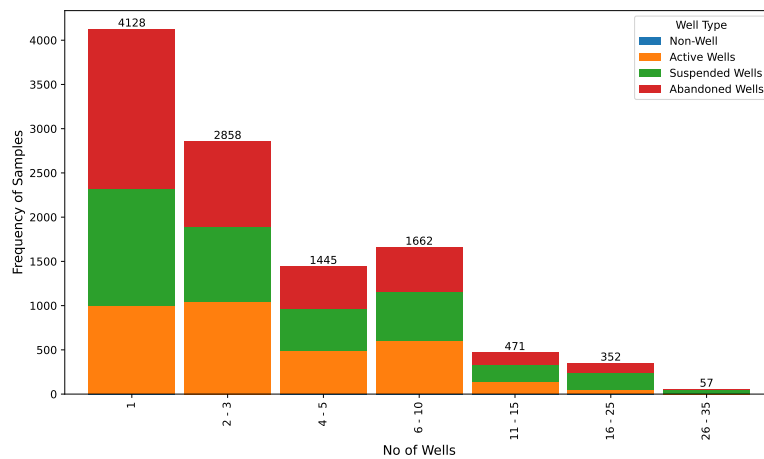
# Alberta Wells Dataset: Pinpointing Oil and Gas Wells from Satellite Imagery



(a) Training set



(b) Validation set



(c) Test set

Figure 5: Distribution of the number of individual wells and the proportion of well types (active, suspended, and abandoned) in positive samples from the dataset. We also include an equal number of images with no wells at all.

Alberta Wells Dataset:  
Pinpointing Oil and Gas Wells from Satellite Imagery

---

Table 11: Test set statistics showing the distribution of image samples by the number of wells per image and the breakdown of well types (active, suspended, and abandoned).

No of Wells in a Image Sample (S)	Test Set				
	Count (Image Samples)	Distribution of Well Type in Samples			
		Total Wells	Active Wells	Suspended Wells	Abandoned Wells
1	4128	4128	999	1325	1804
2 - 3	1242	2858	1042	844	972
4 - 5	328	1445	495	464	486
6 - 10	227	1662	604	555	503
11 - 15	38	471	144	181	146
16 - 25	19	352	56	184	112
26 - 35	2	57	0	56	1
		10973	3340	3609	4024

Table 12: Validation Set statistics showing the distribution of image samples by the number of wells per image and the breakdown of well types (active, suspended, and abandoned).

No of Wells in a Image Sample (S)	Validation Set				
	Count (Image Samples)	Distribution of Well Type in Samples			
		Total Wells	Active Wells	Suspended Wells	Abandoned Wells
1	3393	3393	743	1225	1425
2 - 3	979	2197	833	654	710
4 - 5	190	824	346	248	230
6 - 10	123	910	323	331	256
11 - 15	23	287	67	114	106
16 - 25	11	204	32	63	109
26 - 35	10	300	33	22	245
36 - 55	3	128	29	14	85
		8243	2406	2671	3166

Table 13: Train Set statistics showing the distribution of image samples by the number of wells per image and the breakdown of well types (active, suspended, and abandoned).

No of Wells in a Image Sample (S)	Train Set				
	Count (Image Samples)	Distribution of Well Type in Samples			
		Total Wells	Active Wells	Suspended Wells	Abandoned Wells
1	44299	44299	16715	13116	14468
2 - 3	25378	59190	33099	12706	13385
4 - 5	7899	34544	22456	6321	5767
6 - 10	4927	35333	21522	7796	6015
11 - 15	751	9345	4076	3136	2133
16 - 25	333	6381	1781	2544	2056
26 - 35	67	1994	376	791	827
36 - 55	45	1929	172	777	980
56 - 75	18	1129	86	345	698
76 - 125	1	87	11	63	13
	83718	194231	100294	47595	46342

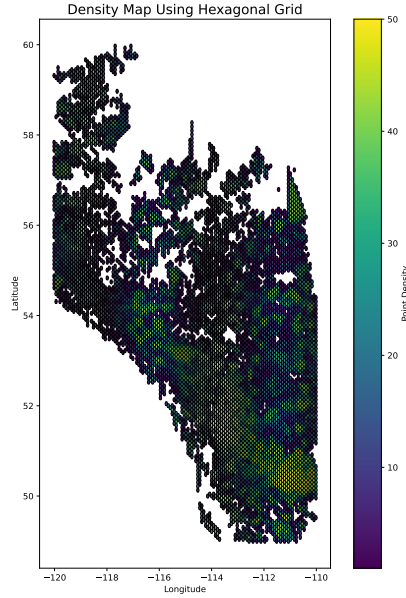
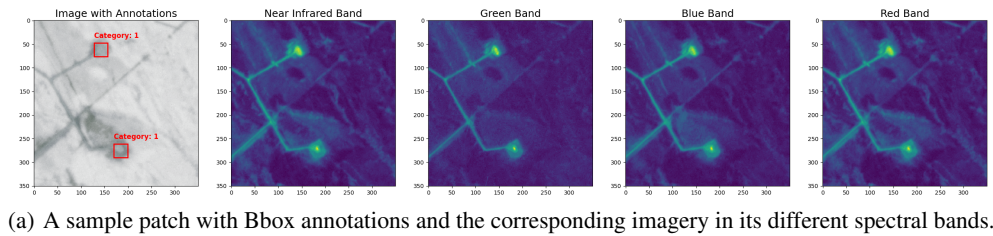


Figure 6: Density map of wells in the Alberta Wells Dataset.

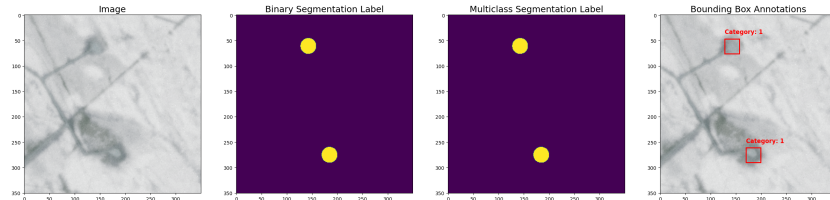
### B.5 PlanetScope Satellite Imagery

For our experiments, we selected a 4-band (RGBN) satellite imagery product (ortho\_analytic\_4b\_sr) from Planet Labs [9] as illustrated in Figure 7. This product uses Planet’s PSB.SD instrument, which features a telescope with a larger 47-megapixel sensor and is designed to be interoperable with Sentinel-2 imagery in several bands. The frequency of each band of image is described in Table 14. The instrument provides a frame size of 32.5 km x 19.6 km, an image capture capacity of 200 million km<sup>2</sup>/day, and an imagery bit depth of 12-bit, with a ground sample distance (nadir) ranging from 3.7 m to 4.2 m.

The satellite images are corrected for atmospheric conditions and spectral response consistency. These multispectral products are tailored for monitoring in agriculture and forestry, offering precise geolocation and cartographic projection. They are ideal for tasks such as land cover classification, with radiometric corrections ensuring accurate data transformation.



(a) A sample patch with Bbox annotations and the corresponding imagery in its different spectral bands.



(b) A sample patch with its segmentation labels (binary and multi-class) and bounding box annotations.

Figure 7: A Sample Patch from the Evaluation Set with 2 active wells.

Table 14: The Frequency of Each Spectral Band of a Planetscope PS.SD acquired Image

Band of Image	Frequency (in nm) of Spectral Band
Band 1 = Blue	465 - 515
Band 2 = Green	547 - 585
Band 3 = Red	650 - 680
Band 4 = Near-infrared	845 - 885

## B.6 Meta Data Description

Each dataset sample is accompanied by metadata, including the sample name (sample ID in string format), the presence of a well in the sample, the number of wells in the sample, and whether a well of a specific category is present in the sample. Table 15 provides an illustration of metadata associated with a sample.

Table 15: Sample of Meta-Data Associated with each Instance in the Dataset

Meta-Data Attribute Name	Value
Sample_Name	eval_6934
wells_present	True
no_of_wells	10
Abandoned_well_present	True
Active_well_present	True
Suspended_well_present	True

## B.7 Label Data Description

For our experiments, we create single-channel segmentation maps, which are binary maps used to locate instances of wells. We also generate multi-class segmentation maps, where each class denotes a well in an active, abandoned, or suspended state. Furthermore, we provide COCO format object detection labels for wells. In both segmentation and detection labels, we represent various states with class IDs as 'Active': 1, 'Suspended': 2, 'Abandoned': 3. To maintain consistency, we standardize the diameter of a well site to 90 meters (typically ranging from 70 to 120 meters) when annotating, resulting in a 30-pixel diameter in the labels. Figure 7(b) illustrates image patches with their corresponding labels, Figure 7(a) illustrates various spectral bands present in an image alongside the original image with bounding box annotations for reference and an example of a bounding box label in COCO format is shown below.

Sample of Bounding Box Annotation:

```
[
  {
    'id': 0,
    'image_id': 'eval_7028',
    'category_id': 1,
    'bbox': [46, 145, 29, 29],
    'iscrowd': 0
  },
  {
    'id': 1,
    'image_id': 'eval_7028',
    'category_id': 2,
    'bbox': [45, 127, 29, 29],
    'iscrowd': 0
  }
]
```

## C Dataset Samples Illustration

Samples from the dataset, covering various scenarios, are shown in Figures 8 and 9.



# Alberta Wells Dataset: Pinpointing Oil and Gas Wells from Satellite Imagery

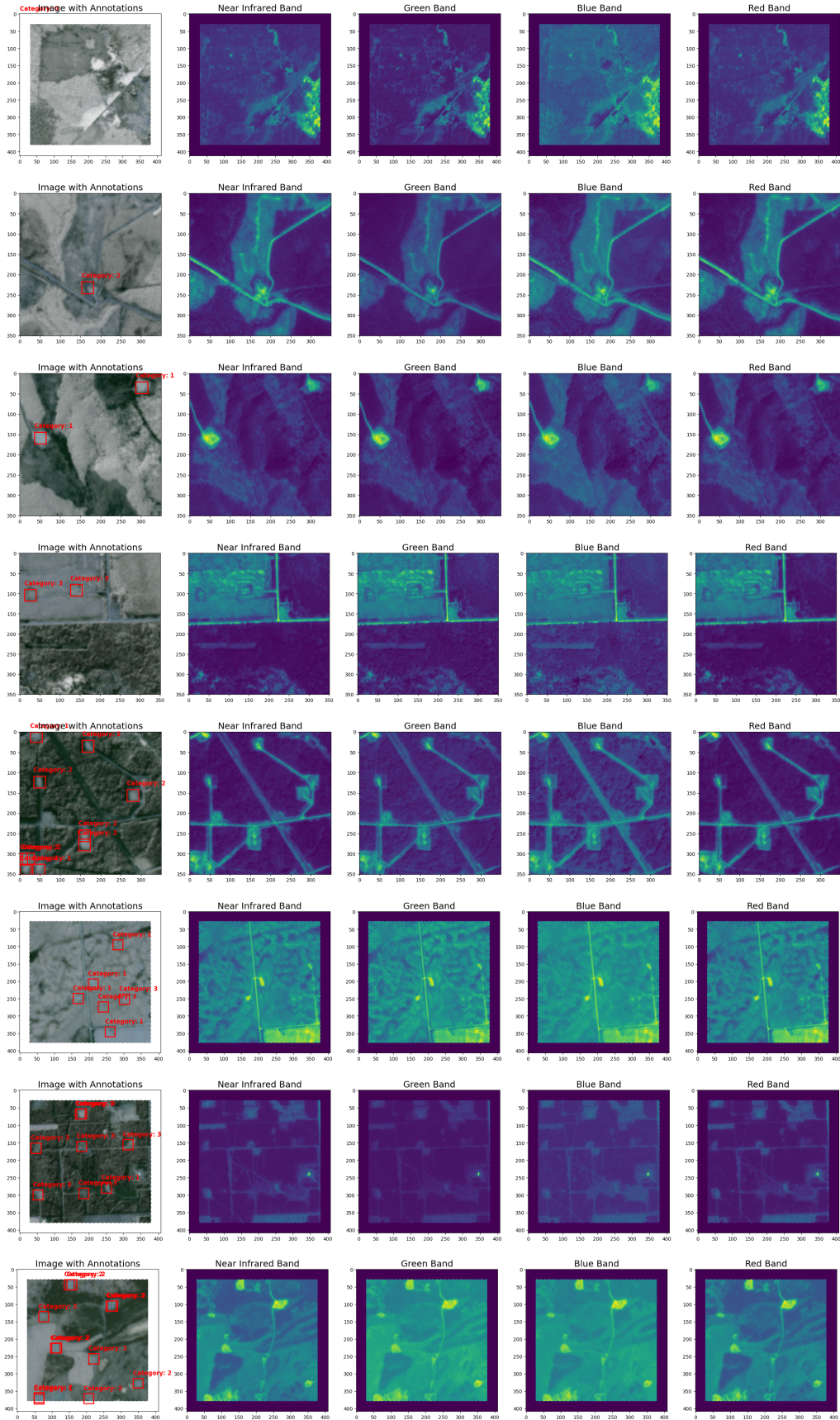


Figure 8: Qualitative results from the dataset illustrate the diverse distribution of wells in dataset samples, including Bbox annotations and corresponding imagery in different spectral bands.

# Alberta Wells Dataset: Pinpointing Oil and Gas Wells from Satellite Imagery

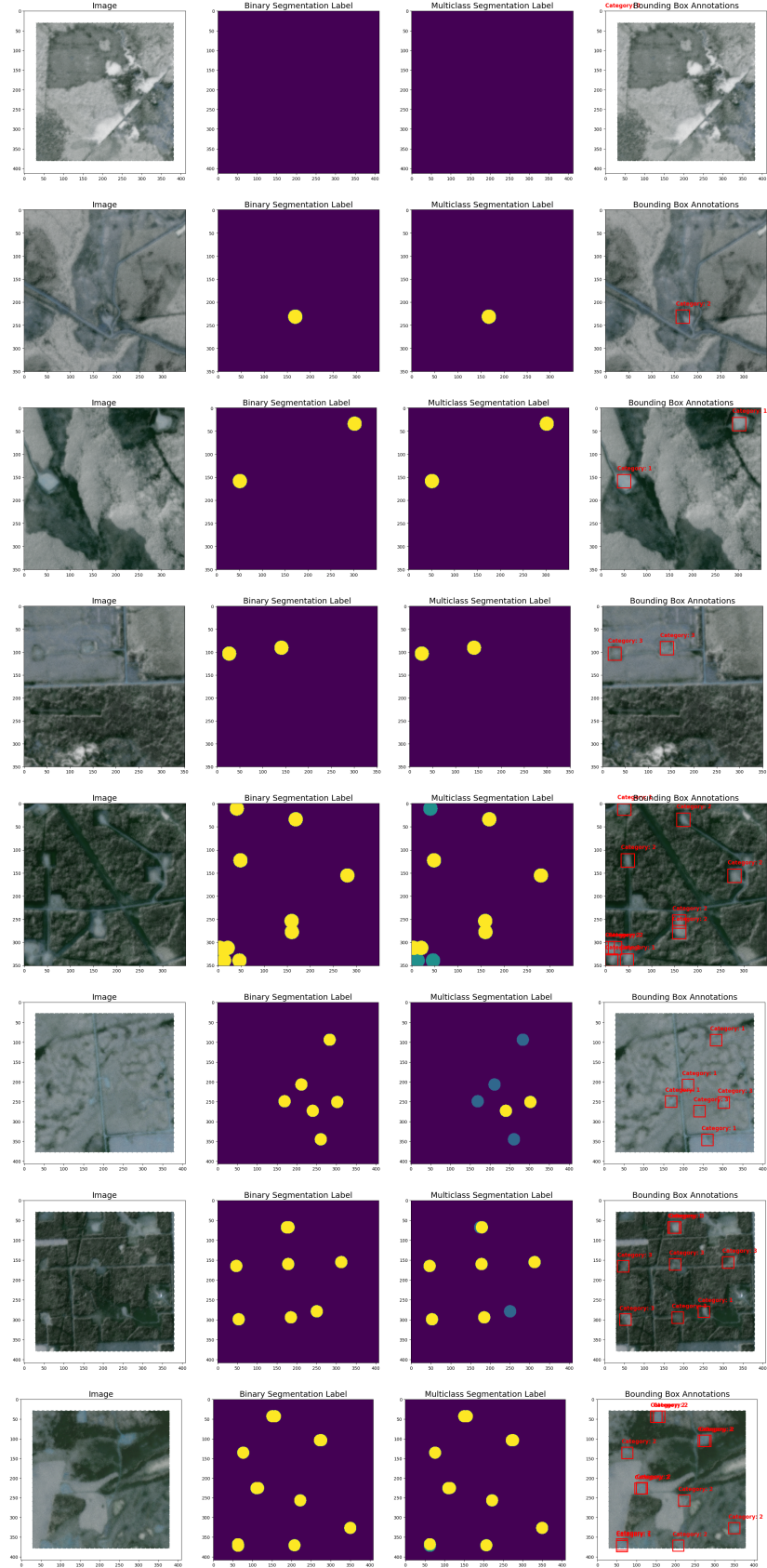


Figure 9: The qualitative results from the dataset showcase the varied distribution of wells in dataset samples, with their corresponding segmentation labels (binary and multi-class) and Bbox annotations.

## D Challenges for ML Community

The Alberta Wells Dataset presents several intriguing challenges for machine learning. Key issues include an imbalanced data distribution, with fewer instances of areas with multiple wells compared to those with single or two wells, and the visual similarity among active, suspended, and abandoned wells, which can confuse standard models. Additionally, varying spatial relationships in the imagery due to varying geography create difficulties for off-the-shelf models. Noise in annotations, even after data quality control and cleaning—such as misclassified wells—further complicates the task. Despite these challenges, the dataset’s large scale and geographical diversity, covering over 213,000 wells, offer significant opportunities for developing robust and generalizable ML models for monitoring oil and gas infrastructure.

## E Documentation frameworks: Datasheet for Datasets

### E.1 Motivation

1. **For what purpose was the dataset created?** Was there a specific task in mind? Was there a specific gap that needed to be filled? Please provide a description.

The Alberta Wells Dataset (AWD) was created to identify oil and gas wells—whether abandoned, suspended, or active—using medium-resolution multi-spectral satellite imagery. While the issue of detecting oil and gas wells has been addressed by several authors, existing datasets are typically small (500-5,000 samples) and limited to specific regions, often including only active wells. This limitation reduces their effectiveness in identifying abandoned or suspended wells. The AWD aims to fill this gap in the literature by offering a comprehensive dataset with over 188,000 samples (including over 94,000 samples containing wells) from PlanetLabs satellite imagery, encompassing more than 213,000 individual wells.

2. **Who created the dataset (e.g., which team, research group) and on behalf of which entity (e.g., company, institution, organization)?**

The raw data is sourced from the Alberta Energy Regulator (AER), specifically from the monthly AER ST37 publication. This dataset includes comprehensive details about all reported wells in Alberta, such as their geographic location, mode of operation, license status, and the type of product extracted, among other attributes. The data is provided in shapefile format along with accompanying metadata. However, the dataset cannot be used directly because the license status or mode of operation often does not reflect the well’s actual status. Therefore, the authors include domain experts from Anonymous, who specialize in field measurements of methane and air pollutant emissions from oil, gas, and urban systems, as well as in the geospatial and statistical data analysis of emissions and energy infrastructure, to ensure the quality of the dataset.

3. **Who funded the creation of the dataset?** If there is an associated grant, please provide the name of the grantor and the grant name and number.

This project was funded by Anonymous.

### E.2 Composition

- **What do the instances that comprise the dataset represent (e.g., documents, photos, people, countries)?**

Are there multiple types of instances (e.g., movies, users, and ratings; people and interactions between them; nodes and edges)? Please provide a description.

We provide a dataset file stored in Hierarchical Data Format 5 (HDF5, i.e., a .h5 file), which contains multispectral 4-band RGBN satellite images in raster format and data labels with both identified by unique instance names. These satellite images, acquired from Planet Labs, have a resolution of 3 meters per pixel and include corresponding metadata. The metadata contains information about the number and types of wells present in a patch. For data labels, we offer binary segmentation maps, multi-class segmentation maps (each class representing a well in an active, abandoned, or suspended state), and COCO format object detection labels. The images were taken from the province of Alberta, Canada, with each satellite imagery patch representing a square with a side length of 1050 meters (1.05 km), covering an area of 1.025 square kilometers. The entire dataset spans over 193,000 square kilometers.

- **How many instances are there in total (of each type, if appropriate)?**

The proposed dataset comprises 188,688 instances, of which 94,344 contain one or more wells, totaling 213,447 well points. Each instance includes corresponding multispectral satellite imagery, segmentation maps (both binary and multi-class, with classes indicating active, suspended, or abandoned states), and bounding box annotations with the state of operations as the object class ID in COCO format. We standardized the diameter of a well site to 90 meters (typically ranging from 70 to 120 meters) for creating annotations, resulting in a

diameter of 30 pixels in the labels. More details about the distribution of wells in each split are provided in the supplementary materials as well as the main paper.

- **Does the dataset contain all possible instances or is it a sample (not necessarily random) of instances from a larger set?** If the dataset is a sample, then what is the larger set? Is the sample representative of the larger set (e.g., geographic coverage)? If so, please describe how this representativeness was validated/verified. If it is not representative of the larger set, please describe why not (e.g., to cover a more diverse range of instances because instances were withheld or unavailable).

The AWD Dataset is based on the AER ST37 monthly status data of wells in the Alberta region of Canada. It includes wells that are in active, suspended, or abandoned states of operation. To ensure the dataset's quality, the authors with appropriate domain expertise conducted extensive quality control, filtering, and duplicate removal. This process was necessary because the full dataset included cases of well sites being restored and reclaimed, as well as various duplicates, noise, and data on other types of wells involving different natural resources. Therefore, the AWD Dataset, which includes multi-spectral satellite imagery, segmentation, and detection labels, is constructed from a refined subset of the original AER ST37 data, specifically targeting oil and gas wells that can be precisely identified.

- **What data does each instance consist of?** "Raw" data (e.g., unprocessed text or images) or features? In either case, please provide a description.

Each Image instance in our dataset, formatted in HDF5, contains satellite imagery represented as a numpy array from Raster Vector. We preprocessed this imagery by reprojecting it to the EPSG 32611 coordinate reference system and removed all geographic metadata, such as image bounds and coordinates, from the shared data. However, we do provide attributes like Sample Name, wells present, no of wells, Abandoned well present, Active well present, and Suspended well present. We utilized Planet Labs' 4-band (RGBN) satellite imagery product (ortho\_analytic\_4b\_sr), which incorporates the latest PSB.SD instrument with a 47-megapixel sensor. Each satellite imagery patch acquired represents a square with a side length of 1050 meters (1.05 km), covering an area of 1.025 square kilometers. The entire dataset spans over 193,000 square kilometers.

- **Is there a label or target associated with each instance?** If so, please provide a description.

There are three types of labeled data for each image: binary segmentation maps (in Rasterio Image format) indicating the presence or absence of oil and gas wells, multiclass segmentation maps (also in Rasterio Image format) potentially identifying various classes of objects, and bounding box annotations (in COCO format) specifying the location and size of objects, such as wells, within the image. These components together form a comprehensive dataset suitable for training and evaluating machine learning models for tasks like object detection and segmentation in satellite imagery, particularly focused on pinpointing oil and gas wells in Alberta.

- **Is any information missing from individual instances?** If so, please provide a description, explaining why this information is missing (e.g., because it was unavailable). This does not include intentionally removed information but might include, e.g., redacted text.

The satellite imagery used in this project was obtained under Planet Labs' [9] Education & Research license, which prohibits sharing raw satellite imagery. We re-projected the raw data to EPSG:32611 using the nearest resampling method and removed all geographic metadata, such as image bounds and coordinates, from the shared data imagery to create a derived product that complies with the license terms.

- **Are relationships between individual instances made explicit (e.g., users' movie ratings, social network links)?** If so, please describe how these relationships are made explicit.

N/A

- **Are there recommended data splits (e.g., training, development/validation, testing)?** If so, please provide a description of these splits, explaining the rationale behind them.

The dataset we propose comprises more than 94,000 patches of satellite imagery containing wells, totaling 188,000 patches sourced from Planet Labs. This dataset covers over 213,000 individual wells. To ensure a balanced dataset, we divided it into training, validation, and testing sets using our algorithm outlined in Section 3.2 of the main paper. Our proposed method for splitting the data aims to create smaller, non-overlapping regions of concentrated wells by clustering patch centroids. These regions are intended to (a) not intersect, (b) be part of a larger geographic area by clustering initial cluster centroids, and (c) contain a similar distribution of non-well patches. This approach ensures that the training, validation, and test sets cover all geographic regions, providing a diverse and thorough evaluation. The dataset splits represent various geographical areas, making it a comprehensive benchmark for evaluation and testing. Each dataset split is stored in an HDF5 format file.

- **Are there any errors, sources of noise, or redundancies in the dataset?** If so, please provide a description. One limitation of our study is our reliance on well locations provided by the Alberta Energy Regulator, which

may not encompass all sites, leading to potential omissions in the ground-truth data. This could result in a lower reported validation and test accuracy, with some correctly predicted well locations being mistakenly categorized as false.

- **Is the dataset self-contained, or does it link to or otherwise rely on external resources (e.g., websites, tweets, other datasets)?** If it links to or relies on external resources, a) are there guarantees that they will exist and remain constant, over time; b) are there official archival versions of the complete dataset (i.e., including the external resources as they existed at the time the dataset was created); c) are there any restrictions (e.g., licenses, fees) associated with any of the external resources that might apply to a dataset consumer? Please provide descriptions of all external resources and any restrictions associated with them, as well as links or other access points, as appropriate.

The dataset does not rely on the persistence of external resources.

- **Does the dataset contain data that might be considered confidential (e.g., data that is protected by legal privilege or by doctor-patient confidentiality, data that includes the content of individuals' non-public communications)?** If so, please provide a description.

No.

- **Does the dataset contain data that, if viewed directly, might be offensive, insulting, threatening, or might otherwise cause anxiety?** If so, please describe why.

No.

### E.3 Collection Process

- **How was the data associated with each instance acquired?** Was the data directly observable (e.g., raw text, movie ratings), reported by subjects (e.g., survey responses), or indirectly inferred/derived from other data (e.g., part-of-speech tags, model-based guesses for age or language)? If the data was indirectly inferred/derived from other data, was the data validated/verified? If so, please describe how.

The AER publishes AER ST37, a monthly list of wells in Alberta, including location, operation mode, license status, and product type. However, the data needs rigorous quality control as license status, or operation mode may not accurately reflect the actual well status. The authors, with extensive domain expertise, removed duplicate well entries in the metadata and shapefile, keeping the most recent update. We then merge and filter the datasets, categorizing wells as active, abandoned, or suspended based on expert criteria. Duplicate coordinates are resolved by keeping the instance with the latest drill date. We verify all wells are within Alberta's boundaries. After thorough quality control by domain experts, we calculate the geographical bounds covered by wells and divide the region into non-overlapping square patches. These patches include varying numbers of wells, with an equal number of patches with and without wells.

- **What mechanisms or procedures were used to collect the data (e.g., hardware apparatus or sensors, manual human curation, software programs, software APIs)?** How were these mechanisms or procedures validated?

We acquired multispectral satellite imagery data from Planet Labs, which comprises four bands (RGBN) with a 3-meter-per-pixel resolution obtained through their proprietary API. This data was processed using quality-controlled and cleaned well data to generate segmentation and object detection annotations. The annotations were created using custom Python code, leveraging libraries like Shapely, GeoPandas, and Rasterio, and were validated through visualization using folium and matplotlib.

- **If the dataset is a sample from a larger set, what was the sampling strategy (e.g., deterministic, probabilistic with specific sampling probabilities)?**

No.

- **Who was involved in the data collection process (e.g., students, crowdworkers, contractors) and how were they compensated (e.g., how much were crowdworkers paid)?**

The dataset was a collaborative effort involving the Alberta Energy Regulator, Planet Labs, and the authors. Without the contributions from individuals in these three organizations, this dataset would not have been possible. Proper credit must be given to the authors, Planet Labs, and the Alberta Energy Regulator when using this data.

- **Over what timeframe was the data collected?** Does this timeframe match the creation timeframe of the data associated with the instances (e.g., recent crawl of old news articles)? If not, please describe the timeframe in which the data associated with the instances was created.

We acquired the data from the Alberta Energy Regulator, specifically from its monthly well bulletin AER ST37 [31], dated March 2024. Leveraging domain expertise, we filtered the data to reflect the condition of wells as of September 30, 2023. This decision was made because imagery acquired from Alberta during the



winter months tends to have high cloud cover. Therefore, we filtered the data to ensure we could collect the best data for each patch based on satellite data acquired between the summer months of June and September in the region.

- **Were any ethical review processes conducted (e.g., by an institutional review board)?** If so, please provide a description of these review processes, including the outcomes, as well as a link or other access point to any supporting documentation.  
N/A

#### E.4 Preprocessing/cleaning/labeling

- **Was any preprocessing/cleaning/labeling of the data done (e.g., discretization or bucketing, tokenization, part-of-speech tagging, SIFT feature extraction, removal of instances, processing of missing values)?** If so, please provide a description.  
In the Dataset section of our submission, we provide a detailed description of the quality control, cleaning, and labeling processes applied to the data obtained from the Alberta Energy Regulator, which forms the basis of our dataset. The satellite imagery utilized in this project was acquired under the Education & Research license from Planet Labs. We reprojected the raw data to EPSG:32611 using the nearest resampling method. Additionally, we removed all geographic metadata, such as image bounds and coordinates, from the shared data imagery to ensure compliance.
- **Was the “raw” data saved in addition to the preprocessed/cleaned/labeled data (e.g., to support unanticipated future uses)?** If so, please provide a link or other access point to the “raw” data.  
The raw satellite imagery data has been saved for internal use; however, it cannot be shared in its current form. Before sharing, the data must undergo preprocessing to remove metadata, as stipulated by the agreement mentioned earlier.
- **Is the software that was used to preprocess/clean/label the data available?** If so, please provide a link or other access point.  
We plan to share the relevant code used for dataset quality control, patch creation, dataset splitting, data acquisition, and label and HDF5 file creation with the public release of the dataset in the future.
- **Any other comments?**  
N/A

#### E.5 Uses

- **Has the dataset been used for any tasks already?** If so, please provide a description.  
Currently, there are no public demonstrations of the AWD Dataset in use. In this work, we showcase its application for Binary Segmentation and Binary Object Detection of Well Sites to train algorithms for accurately locating well sites. These algorithms can be scaled across larger regions of interest to compare against existing databases, identifying potentially undocumented wells. Flagging wells not present in databases is crucial, as these could be abandoned wells that are significant emitters of greenhouse gases, making them candidates for plugging.
- **Is there a repository that links to any or all papers or systems that use the dataset?** If so, please provide a link or other access point.  
N/A
- **What (other) tasks could the dataset be used for?**  
Additionally, we provide multi-class labels indicating the operational state of the wells for both cases. These labels can be utilized in future projects for locating wells and classifying their operational status, which will aid in identifying well sites that are not present in government records.
- **Is there anything about the composition of the dataset or the way it was collected and preprocessed/cleaned/labeled that might impact future uses?**  
This dataset focuses on Alberta, Canada, known for its diverse oil reserves and varied landscapes, providing a representative sample comparable to regions in the Appalachian and Mountain West areas of the United States and some former Soviet states with oil wells and unidentified site issues. A limitation of our study is the reliance on well locations from the Alberta Energy Regulator, which may miss some sites, leading to potential false negatives in the ground-truth data. However, this should have minimal impact on algorithm training, as these labels are a minor part of the dataset, and deep learning algorithms can handle moderate label noise well (see e.g., [48]). The main effect may be underreported test accuracy, with some correctly predicted well locations wrongly counted as false. We plan to investigate this further in future work. Additionally, the use of

multi-spectral optical data in the AWD dataset may limit the models' applicability in regions with frequent cloud cover.

- **Are there tasks for which the dataset should not be used?** If so, please provide a description.  
This dataset is intended for non-commercial use only and should not be utilized in any application that could negatively impact biodiversity.
- **Any other comments?**  
N/A

## E.6 Distribution

- **Will the dataset be distributed to third parties outside of the entity (e.g., company, institution, organization) on behalf of which the dataset was created?** If so, please provide a description.  
Yes, the dataset will be made public (open-source) in the future.
- **How will the dataset will be distributed (e.g., tarball on website, API, GitHub)?** Does the dataset have a digital object identifier (DOI)?  
The dataset is accessible through Zenodo.
- **When will the dataset be distributed?**  
The Dataset is made public and hosted on Zenodo at [https://github.com/RolnickLab/Alberta\\_Wells\\_Dataset](https://github.com/RolnickLab/Alberta_Wells_Dataset).
- **Will the dataset be distributed under a copyright or other intellectual property (IP) license, and/or under applicable terms of use (ToU)?** If so, please describe this license and/or ToU, and provide a link or other access point to, or otherwise reproduce, any relevant licensing terms or ToU, as well as any fees associated with these restrictions.  
The AWD Dataset is released under a Creative Commons Attribution-NonCommercial 4.0 International (CC BY-NC 4.0) License (<https://creativecommons.org/licenses/by-nc/4.0/>).
- **Have any third parties imposed IP-based or other restrictions on the data associated with the instances?** If so, please describe these restrictions and provide a link or other access point to, or otherwise reproduce, any relevant licensing terms, as well as any fees associated with these restrictions.  
The satellite imagery used in this project was acquired under the Education & Research license of Planet Labs [9]. This license allows for the use of the data in publications and the creation of derivative products, which can be shared in association with publications. However, raw imagery cannot be shared publicly. To comply with these guidelines, we share the data in HDF5 format, with satellite imagery represented as a numpy array from Raster Vector. We have removed all geographic metadata, such as image bounds and coordinates, from the shared data. The data is intended for academic use only and should not be used for commercial purposes. Proper credit must be given to the current authors, Planet Labs, and the Alberta Energy Regulator when using this data.
- **Do any export controls or other regulatory restrictions apply to the dataset or to individual instances?** If so, please describe these restrictions, and provide a link or other access point to, or otherwise reproduce, any supporting documentation.  
No
- **Any other comments?**  
N/A

## E.7 Maintenance

- **Who is supporting/hosting/maintaining the dataset?**  
The dataset is hosted on Zenodo.
- **How can the owner/curator/manager of the dataset be contacted (e.g., email address)?**  
You can reach the authors through the email addresses provided in the paper. Additionally, you can raise any issues on the GitHub repository, which will be made public in the future.
- **Is there an erratum?** If so, please provide a link or other access point.  
Not to the best of our knowledge.
- **Will the dataset be updated (e.g., to correct labeling errors, add new instances, delete instances)?** If so, please describe how often, by whom, and how updates will be communicated to users (e.g., mailing list, GitHub)?  
As our dataset is based on data from a fixed timeframe and consists of satellite imagery collected during a

specific period, we do not currently have plans to update it in the near future. However, if there are any changes to these plans, updates to the dataset will be posted on the corresponding GitHub repository once it is made public.

- **Will older versions of the dataset continue to be supported/hosted/maintained?** If so, please describe how. If not, please describe how its obsolescence will be communicated to users.  
If there are newer versions of the dataset, they will maintain the same format. We will ensure that the code associated with the project on GitHub supports these updates, and we will update the READMEs to reflect any changes to the dataset.
- **If others want to extend/augment/build on/contribute to the dataset, is there a mechanism for them to do so?** If so, please provide a description. Will these contributions be validated/verified? If so, please describe how. If not, why not? Is there a process for communicating/distributing these contributions to users? If so, please provide a description.  
We plan to share the relevant code in the future. However, to ensure the ability to compare against our results, we encourage those who wish to build on the dataset to publish their work separately rather than adding to our data repository.
- **Any other comments?**  
N/A